2016

Exchange-coupling behavior in nanostructured FePt/Fe bilayer films

Yi Liu
University of Nebraska-Lincoln, yliu@unl.edu

David J. Sellmyer
University of Nebraska-Lincoln, dsellmyer@unl.edu

Exchange-coupling behavior in nanostructured FePt/Fe bilayer films

Y. Liu and D. J. Sellmyer
Nebraska Center for Materials and Nanoscience and Department of Physics and Astronomy, University of Nebraska, Lincoln, NE 68588, USA

(Presented 15 January 2016; received 6 November 2015; accepted 21 December 2015; published online 2 March 2016)

Different thicknesses of FePt/Fe bilayer films are deposited on (001) MgO substrates by sputtering Fe and Pt targets with *in-situ* heating at 830^{O}C. X-ray diffraction indicates a complete alignment of the FePt [001] axis with MgO [001] axis. The nucleation field H_n is estimated from hysteresis loops measured using a SQUID magnetometer. A FePt/Fe bilayer model is proposed to calculate the nucleation field H_n and compared with the experimental data. The model can explain experimental trends and gives useful predictions for nanostructure synthesis and further experiment. [http://dx.doi.org/10.1063/1.4943414]

I. INTRODUCTION

The maximum achievable energy product of a permanent magnetic material is determined by its saturation magnetization M_s and its magnetic anisotropy K. In particular, it is always true that $(BH)max \leq (4\pi M_r)^2/2 \leq (4\pi M_s)^2/2$, where M_r is the remanent magnetization. The principle of exchange-coupled magnets is to use the properties of a hard- and a soft-phase nanocomposite to increase M_s and energy product.[1–6] Recently Jiang and Bader investigated the effect of various geometries of the hard- and soft-phases in an exchange-coupled magnet.[7] The M_s of the composite is $M_{sc}=f_h M_h+f_s M_s$ where f_h denotes the volume fraction of the hard-phase and f_s the volume fraction of the soft-phase. Naturally, M_{sc} can be increased by adding a large volume fraction of the soft-phase. However, as the volume fraction of the soft-phase increases, the size and the number of the soft-phase grains will increase, which causes a drop of coercivity. It is shown by theory that the diameter of the soft-phase must not exceed twice the domain wall thickness of the hard-phase.[2] An optimum of the volume fraction of the soft-phase for maximum energy product can be identified by experimental work. Recently, the authors investigated Fe-Pt based nanostructured magnets by varying the Fe content from 59.4at% to 64at%. The resulting two phases were identified as a hard phase $L1_0$ FePt and a soft-phase *fcc* Fe(Pt).[8] The easy axis of the hard-phase $L1_0$ FePt is aligned by deposition on a (001) MgO single crystal. A high nominal energy product up to 54 MGOe corresponding to a film composition $Fe_{64}Pt_{36}$, and soft-phase volume fraction of 16% was achieved. Further increase in Fe concentration and soft-phase volume fraction resulted in a decrease of coercivity and maximum energy product. The volume fraction of 16% is rather small and one would like to investigate whether further increase in the soft-phase volume fraction can increase the M_{sc} and maximum energy product. This paper reports our recent experimental and theoretical results on FePt/Fe bi-layer exchange-coupled nanomagnets. Both the FePt layer and Fe layer thicknesses are varied to cover a large range for comparison with model calculations.

II. EXPERIMENTAL PROCEDURE

The FePt/Fe films were deposited on (001) oriented single-crystal MgO substrates in an AJA International sputtering system with *in-situ* heating at 830°C. The sputtering rate of Fe and Pt were adjusted for co-sputtering to realize FePt layers or Fe layers with different thicknesses. The

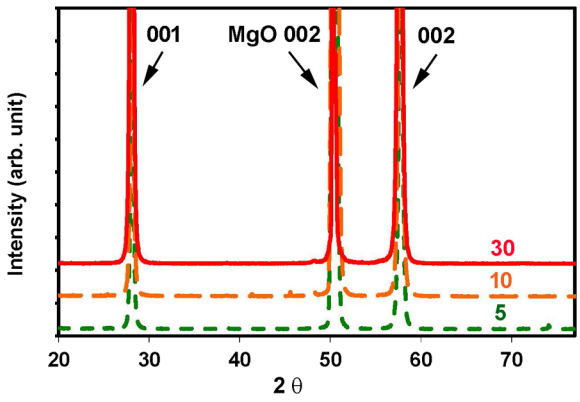

FIG. 1. X-ray diffraction patterns of FePt films on MgO substrate.

compositions were calculated from the sputtering rates of Fe and Pt, which were determined by X-ray reflectivity measurements of the film thickness. Before each deposition, a vacuum of better than $4x10^{-8}$ Torr was achieved. The Ar pressure during deposition was 5 mTorr. The films were characterized using a Rigaku x-ray diffractometer and a JEOL 2010 transmission electron microscope. The magnetic properties were measured using a Quantum Design SQUID magnetometer up to a maximum applied field of 70 kOe at room temperature. SQUID measurement was performed at room temperature with magnetic field applied perpendicular to the film plane ($\perp$).

III. RESULTS AND DISCUSSION

The alignment of the easy axis of FePt is confirmed by X-ray diffraction as shown in Figure 1. Only three strong peaks are observed: FePt (001), FePt (002), and MgO (002), indicating a perfect alignment of FePt (001)// MgO (002). Figure 2 shows the hysteresis loops of 5 nm FePt films deposited on MgO substrates. The thicknesses of the Fe layers are 0 nm, 0.75 nm, 1.5 nm and 2.0 nm as shown in the figure. Figure 3 shows the hysteresis loops of 10 nm FePt films deposited on MgO substrates. The Fe layer thicknesses are 0 nm, 1 nm, 2 nm, and 3 nm as shown in the figure. The hysteresis loops of 30 nm FePt films deposited on MgO substrates are shown in Figure 4. The thicknesses of the Fe layers are 0 nm, 6 nm, 12 nm, and 18 nm as shown in the figure. The nucleation field is defined by the field at which the magnetization is starting to drop quickly as indicated by an arrow. Thus, the nucleation field is always smaller than the coercivity H_c. For all FePt films, the coercivity and nucleation field decreases, and saturation magnetization increases with Fe thickness. The energy product $(BH)_{max}$ shows a maximum and then decreases with Fe layer thickness. For the same thickness of Fe layer, thick FePt film shows higher coercivity and nucleation field than thinner FePt film.

An earlier model[2] has predicted a flat nucleation field for small soft-phase embedded in a hard-phase when the size of the soft-phase is smaller than twice the domain wall thickness of the hard-phase. In our case, the soft-phase is on top of the hard-phase and some are very thin, thinner than the domain-wall thickness of 3.9 nm of FePt. We therefore performed an analysis on the magnetic reversal process.

In our earlier work, we found that the FePt films deposited on MgO substrate are composed of isolated FePt crystals.[8] We expect the Fe layer deposited on top of FePt will inherit similar structure. Figure 5 shows a proposed FePt/Fe model. The initial magnetization of both layers is upward after saturation as shown in Figure 5(a). Then an opposite field H_a is applied and increased gradually. When the applied field H_a is increased to the nucleation field H_n, the magnetization of the Fe layer is reversed and a domain-wall of FePt layer separating the reversed Fe layer and non-reversed layer FePt is created as shown in Figure 5(b). The free energy change in this process is

$$\Delta G = -2 \int_{soft-} (H_a - H_h) M_s dV - \int_{dom} (H_a - H_b + H_s) M_h dV + K_h V_h \quad (1)$$

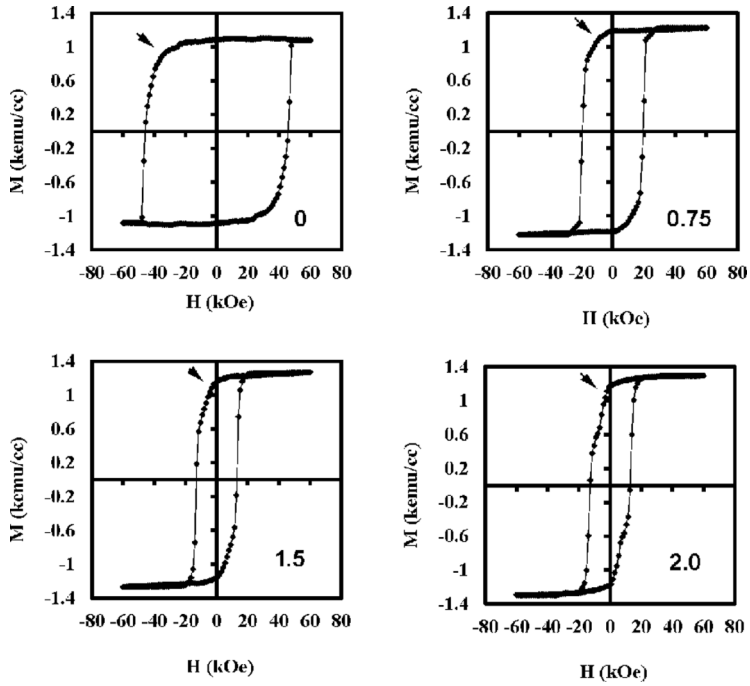

FIG. 2. Hysteresis loops of 5 nm FePt films deposited on MgO substrates. The thicknesses of the Fe layers are 0 nm, 0.75 nm, 1.5 nm and 2.0 nm as shown in the figure.

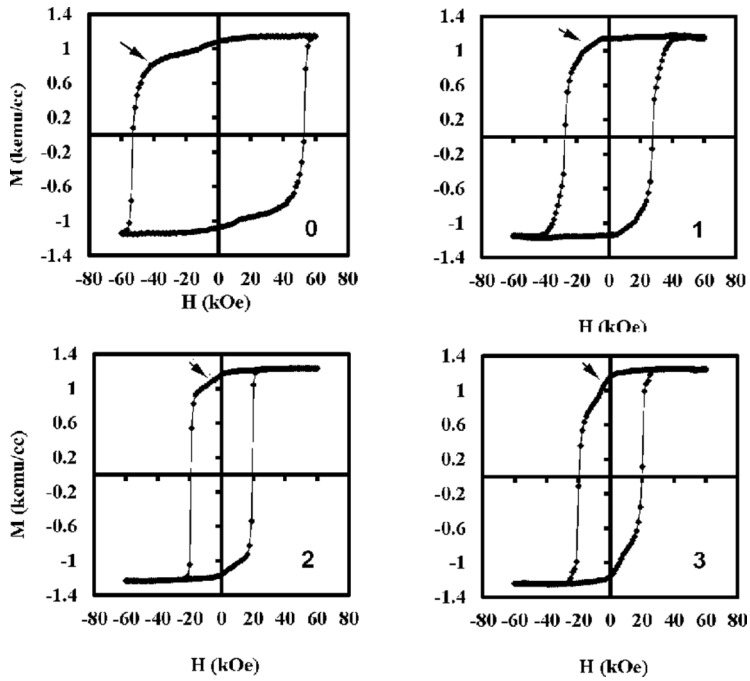

FIG. 3. Hysteresis loops of 10 nm FePt films deposited on MgO substrates. The thicknesses of the Fe layers are 0 nm, 1 nm, 2 nm, and 3 nm as shown in the figure.

where the integration (soft) is over the Fe layer, integration (dom) is over the domain-wall layer. H_h is the magnetic field from the whole FePt layer, H_b is the field from the FePt layer below the domain layer, H_s is the field from the Fe layer. M, V and K are the saturation magnetization, volume and anisotropy, respectively. Subscripts h and s indicate the hard-layer FePt and soft-layer Fe,

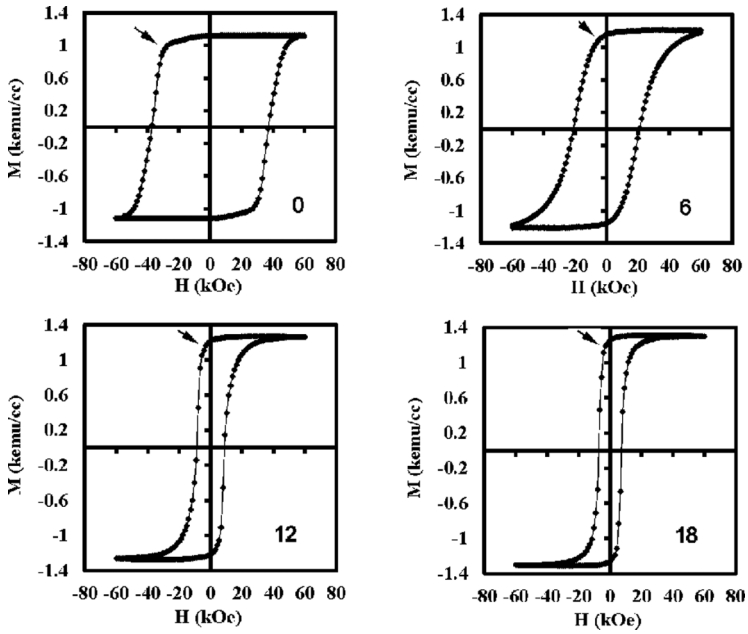

FIG. 4. Hysteresis loops of 30 nm FePt films deposited on MgO substrates. The thicknesses of the Fe layers are 0 nm, 6 nm, 12 nm, and 18 nm as shown in the figure.

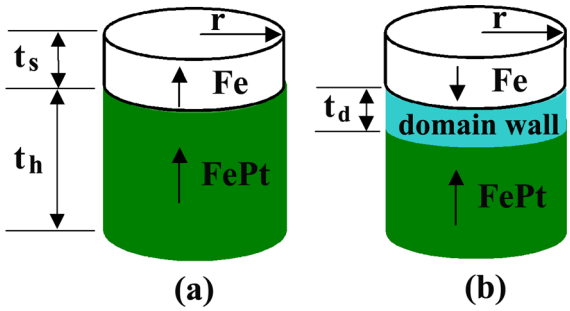

FIG. 5. The proposed bicrystal model. The sizes of FePt and Fe layers are shown in the figure.

respectively. At zero applied field, Figure 5(a) is stable. As the applied field increases, Figure 5(a) becomes unstable and Figure 5(b) becomes stable at a particular applied field H_n. ΔG changes from positive to negative as applied field increases. The transformation happens under the condition of $\Delta G<0$. Assuming the applied field H_a is uniform, the nucleation field H_n is deduced by letting $\Delta G=0$

$$H_n = \frac{2M_s \int_{\text{soft}} H_h dV + M_h \int_{dom} H_b dV - M_h \int_{dom} H_s dV + K_h V_d}{2M_s V_s + M_h V_d} \tag{2}$$

where V_d is the volume of the domain-wall defined by $V_d = At_d$, A is the cross section, t_d is the thickness of the domain-wall as shown in Figure 5(b). t_d can be found by $d\Delta G/dt_d = 0$. The magnetic properties input data for the calculation are: M_h =1140 emu/cm^3, M_s =1700 emu/cm^3, K_h = 65 Merg/cm^3. The calculation of integrals yields H_n as a function of the thickness, diameter and magnitization of the FePt and Fe layers.

Figure 6 shows H_n and its four components in Equation (2) for 10 nm FePt as an example. The first term is due to the interaction between the FePt layer and the Fe layer. It starts from 0 at $t_s = 0$ and increases, reaching a maximum and then decreases slowly. The second term is the interaction between the bottom FePt layer and the domain layer shown in Figure 5(b). It starts around 5 kOe

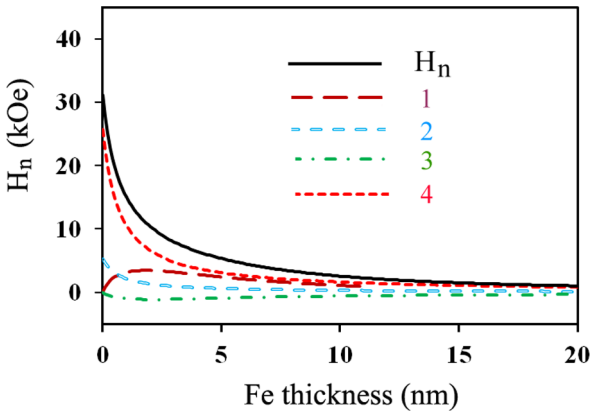

FIG. 6. The nucleation field and its 4 contributing components for 10 nm FePt.

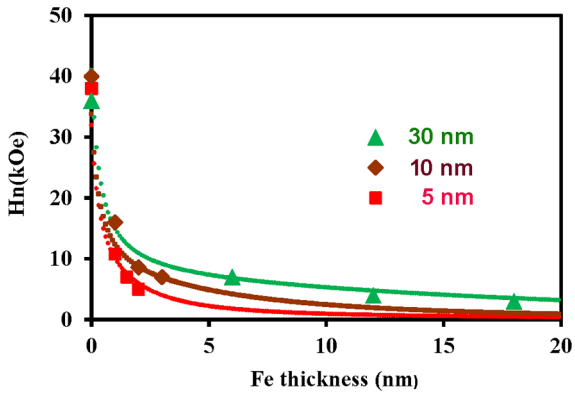

FIG. 7. The nucleation fields as a function of Fe thickness. The thicknesses of FePt layer are 5 nm, 10 nm and 30 nm as shown in the figure.

depending on the size of FePt and decreases slowly with t_s. The third term is the interaction between the Fe layer and the domain layer. It starts from 0 at $t_s = 0$, and has negative value as t_s increases, showing that it reduces the nucleation field. The fourth term is due to the anisotropy of the FePt layer and decreases rapidly with increasing Fe thickness.

The nucleation field from Equation (2) is calculated for 5 nm FePt, 10 nm FePt and 30 nm FePt and is shown in Figure 7 in comparison with experimental data from this work. The calculated H_n is in agreement with the experimental data in the following two features: Firstly, the model predicts that H_n decreases with increasing thickness of the soft-layer. Secondly, for the same thickness of the soft-layer, the 30 nm FePt layer has higher H_n. For most films, the experimental H_n is slightly lower than the calculated H_n. This could be caused by the inter-diffusion between the Fe layer and FePt layer, which will lower the anisotropy of FePt and expand the size of the Fe layer. The anisotropy decrease of FePt with film thickness was also observed in the data of Shima *et al.*[9] Although the authors did not discuss anisotropy in their paper, their hysteresis loop shows a significant drop of coercivity in the 3 nm thick FePt film.

Synthesizing an exchange-coupled nano-magnet requires one to choose the hard- phase, the soft-phase, and design the sizes of both hard-phase and soft-phase to produce a favorable nanostructure. A model will provide a guide to find what processing parameters and geometries of the hard-phase and soft-phase are most suitable to realize the optimum nanostructure and maximum energy product. Now we estimate the energy product $(BH)_{\max}$ using our model. To achieve maximum energy product the nucleation field must be large such that $H_n > 2\pi M_s$, and $(BH)_{max}$ is estimated by $(2\pi M_s)^2$. For $H_n < 2\pi M_s$, $(BH)_{max}$ is estimated by $(4\pi M_s - H_n)H_n$. Figure 8 shows $(BH)_{max}$ for different thickness FePt films as a function of Fe layer thickness. For each FePt thickness, a

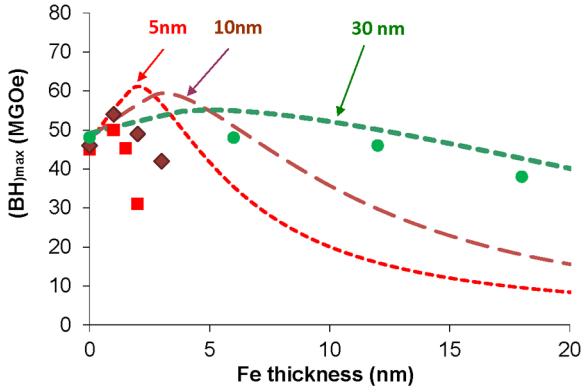

FIG. 8. Comparison of calculated and experimental energy product of FePt:Fe bicrystals as a function of Fe thickness. The thicknesses of FePt layer are 5 nm, 10 nm and 30 nm as shown in the figure.

maximum $(BH)_{max}$ appears at a critical Fe layer thickness t_{sc}. For Fe layer thinner than t_{sc}, $(BH)_{max}$ decreases because the overall M_{sc} of the FePt/Fe film decreases. For Fe layer thicker than t_{sc}, $(BH)_{max}$ decreases because H_n drops drastically. $(BH)_{max}$ among all the FePt thicknesses appears at the thinnest FePt layer structure where the FePt can sustain its $L1_0$ structure and its anisotropy. In reality, it has been found that the anisotropy of $L1_0$ structure FePt shows significant drop in anisotropy when the FePt thickness is below 4 nm and the $(BH)_{max}$ is much lower than the prediction. Another obstacle in achieving the $(BH)max$ is the inter-diffusion between the Fe layer and FePt layer, which lowers both the anisotropy of the FePt layer and the saturation magnetization of Fe layer. Nevertheless, both the model and experimental data identify an optimum FePt thickness t_o for $(BH)_{max}$: below t_o anisotropy of FePt layer drops, Above t_o, H_n decreases.

IV. CONCLUSIONS

In summary, we have investigated the exchange coupling behavior of FePt/Fe bilayer films and proposed a simple model for prediction of nucleation field and energy product for the bilayer structure FePt/Fe. This model employs the properties and sizes of both FePt layer and Fe layer and gives three useful predictions: (1) The highest energy product in a hard-soft- nano-composite can be achieved at the smallest size of the hard-phase where the anisotropy of the hard-phase does not decrease with its size. (2) For a constant thickness of Fe layer, the nucleation field H_n increases with increasing thickness of FePt, assuming a constant anisotropy of FePt. (3) For a constant thickness of FePt layer, an optimum thickness of Fe exists. The experimental optimum thickness is lower than the model prediction due to inter-diffusion between FePt layer and Fe layer.

ACKNOWLEDGEMENT

This research is supported by ARO (WF911NF-10-2-0099). The work was performed in part in the Nebraska Nanoscale Facility, Nebraska Center for Materials and Nanoscience, part of the National Nanotechnology Coordinated Infrastructure, which is supported by the National Science Foundation under Award ECCS-1542182 and the Nebraska Research Initiative.

[1] E.F. Kneller and R. Hawig, IEEE Trans. Magn. **27**, 3588 (1991).
[2] R. Skomski and J.M.D. Coey, Phys. Rev. B **48**, 15812 (1993).
[3] D.J. Sellmyer, Nature **420**, 374 (2002).
[4] J. P. Liu, C.P Luo, Y. Liu, and D.J. Sellmyer, Appl. Phys. Lett. **72**, 483 (1998).
[5] W. Liu, Y. Liu, R. Skomski, and D.J. Sellmyer, in *Advanced Magnetic Materials I: Nanostructural effects*, edited by Y. Liu, D.J. Sellmyer, and D. Shindo (Springer, Berlin, 2006), p. 182.
[6] C. Rong, H. Zhang, X. Du, J. Zhang, S. Zhang, and B. Shen, JAP. **96**, 3921 (2004).
[7] J. S. Jiang and S. D. Bader, J. Phys: Condens. Matter **26**, 064214 (2014).
[8] Y. Liu, T. Gorge, R. Skomski, and D.J. Sellmyer, Appl. Phys.Lett. **99**, 172504 (2011).
[9] T. Shima, K. Takanashi, Y. K. Takahashi, and K. Hono, Appl. Phys. Lett. **85**, 2571 (2004).